Journal of Materials Chemistry A

Distinguishing photo-induced oxygen attack on alkyl chain versus conjugated backbone for alkylthienyl-benzodithiophene (BDTT)-based push-pull polymers

Journal:	*Journal of Materials Chemistry A*
Manuscript ID	TA-ART-06-2023-003256.R1
Article Type:	Paper
Date Submitted by the Author:	20-Jul-2023
Complete List of Authors:	Anderson, Michael; University of Arizona, Materials Science and Engineering Hamstra, Anna; University of Arizona, Department of Chemistry and Biochemistry Larson, Bryon; National Renewable Energy Laboratory Ratcliff, Erin; University of Arizona, Department of Chemical and Environmental Engineering

ARTICLE

Distinguishing photo-induced oxygen attack on alkyl chain versus conjugated backbone for alkylthienyl-benzodithiophene (BDTT)-based push-pull polymers

Received 00th January 20xx,
Accepted 00th January 20xx

DOI: 10.1039/x0xx00000x

Michael A. Anderson,[a] Anna Hamstra,[b] Bryon W. Larson[c] and Erin L. Ratcliff *[abd]

Synthetic design has enabled increasing power conversion efficiency advances in organic photovoltaics (OPV). One continuing knowledge gap is detailed understanding of single-material chemical (photo)stability. Many considerations are based on prior OPV-relevant donor homopolymer systems rather than the next-generation push-pull architectures. Generally, energetic offsets between the lowest occupied molecular orbital of the donor and molecular oxygen are assumed to dictate kinetics of photo-induced charge transfer to a super oxide radical. Herein we determine the ambient-induced photo-degradation pathways, presented as proposed site-specific arrow-pushing mechanisms, for five donor polymers all containing the same push unit - alkylthienyl-substituted-benzodithiophene (BDTT) - but with chemically distinct pull units. The donor-only polymer films were subject to controlled photobleaching in air as an accelerated degradation approach, coupled with simultaneous monitoring of absorptance. Sample subsets were periodically removed and analyzed with x-ray photoelectron spectroscopy, to evaluate near-surface chemical composition and oxygen additions to hetero reporter atoms on either the BDTT push unit or distinct pull unit (i.e, sulphur and nitrogen). This methodology allows us to distinguish between different mechanisms of bond cleavage and formation. Overall, we find that neither polymer redox properties nor individual push or pull unit stabilty are sufficient to predict photo-oxidative degradation of these polymers. Rather, there is a greater dependence on the susceptibility of unique structural groups within a polymeric system. Alkyl chain oxygen addition is generally the first attack site and direct sulfur oxidation on the conjugated backbone occurs after saturation of the alkyl chain initiation sites. This work provides a standard that could be used to evaluate relative photo-oxidative (in)stability for new OPV materials quickly – prior to time-consuming device optimization - and demonstrates an effective methodology for correlating optical degradation with chemical structure alterations via spectroscopic signatures to guide synthetic design.

1. Introduction

The development of photostable organic-based opto-electronic materials depends critically on knowledge of the primary factors that cause instability and the relevant degradation pathway(s). This is especially true for modern organic photovoltaic (OPV) materials that utilize increasingly complex push-pull architectures to achieve performance enhancements. These material constructs enable fine tuning of the energetics of charge carriers and reduction of exciton binding energies in both donor and acceptor materials.[2-5] Collectively these materials have greatly improved the understanding of the photophysics responsible for recent increases in OPV performance. [6-9]

One predominant example is the structural evolution of push-pull donor polymers containing an alkylthienyl-substituted-benzodithiophene (BDTT) push unit. Pull units include diketopyrrolopyrrole (DPP),[10] ethylhexylfluorothienothiophene (EFT),[11] fluorobenzotriazole (FTAZ) [21] thienopyrroledione (TPD), [12, 13] and benzodithiophenedione (BDD).[14] All five co-polymers are D-A architectures, rather than randomized block co-polymers, collectively summarized in **Figure 1a**. This class of BDTT donor polymers represent historic synthetic approaches to optimize charge transport, microstructure, and optical properties. The BDTT unit (*PBDTT*- in **Figure 1a**, left) was first developed for polymer solar cells by Huo et al. in 2010 as a structural modification to the benzodithiophene (BDT) unit, yielding increased aggregation and lower bandgaps. [15, 16] Incorporating the pull units, PBDTT-DPP has been demonstrated to have high charge mobilities in highly ordered polymer films.[17-19] Increased OPV device performance was observed over the BDT polymer (PBDT-DPP) due to higher mobilities (attributed to increased order) and increased device voltages (attributed to transport levels further from vacuum).[19] PBDTT-DPP has demonstrated a

[a] *Department of Materials Science and Engineering, University of Arizona, Tucson, AZ 85721.*
[b] *Department of Chemistry and Biochemistry, University of Arizona, Tucson, Arizona 85721.*
[c] *Chemistry and Nanoscience Center, National Renewable Energy Laboratory, Golden, CO 80401.*
[d] *Department of Chemical and Environmental Engineering, University of Arizona, Tucson, AZ 85721.*
† Footnotes relating to the title and/or authors should appear here.
Electronic Supplementary Information (ESI) available: [details of any supplementary information available should be included here]. See DOI: 10.1039/x0xx00000x

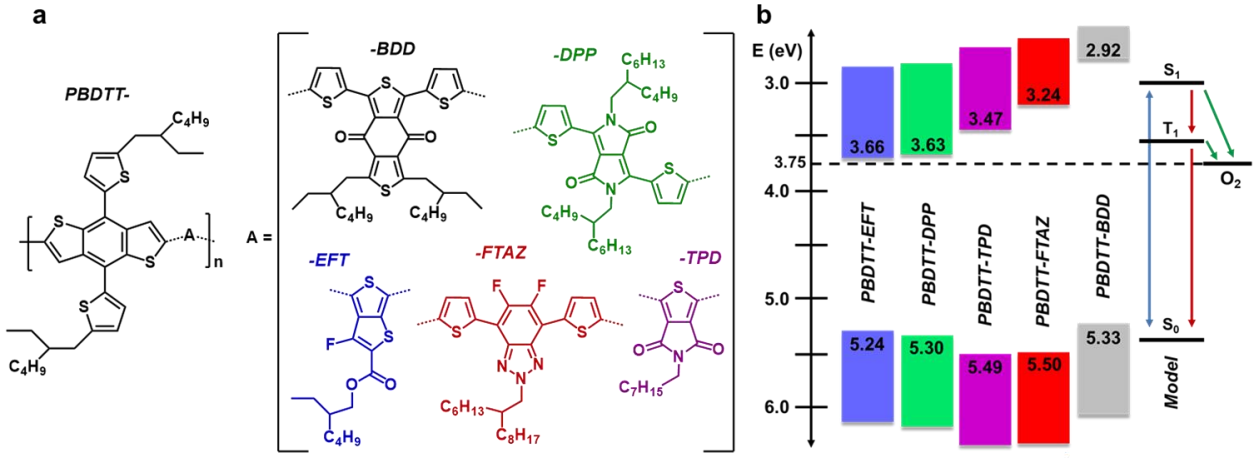

Figure 1. a) Chemical structures and **b)** redox properties of the five push-pull polymer donors that all share the BDTT (push) unit. O_2 electron affinity from Hoke et al. [1] Further details on the polymers including alternate names, full chemical names, and the sources for redox level properties are given in **Table S1**.

device efficiency of 6.5%. [19] PTB7-Th (PBDTT-EFT) also has literature precedent and structurally evolved from an original BDT-based polymer, PTB7. [20, 21] OPV performance was similarly improved due to redshifted absorption and increased coplanarity/aggregation.[22, 23] The optimization of PTB7-Th-based devices brought OPV efficiency over 10% in 2015, [24] a significant milestone in reaching the "10 and 10" efficiency and lifetime goals commonly thought to indicate market viability for OPV. Both PBDTT-FTAZ and PBDTT-TPD introduced unique pull groups to promote planarity, with PBDTT-FTAZ reporting device efficiencies c.a. 5%. [16, 25] PBDTT-TPD showed only modest OPV performance with PCBM yet achieved a 6.6% PCE in an all-polymer flexible cell [24] Finally, PBDTT-BDD, [14] more commonly called PBDB-T, which was the first in a family of PBDB-T-based polymers (including the fluorinated (-2F) derivative abbreviated PM6) that have demonstrated device efficiencies over 19%.[9, 26, 27]

Despite these applied advances, there is still a fundamental knowledge gap relating push-pull structural design to intrinsic photostability. This gap needs to be addressed to produce materials achieving sufficient performance, cost, and stability metrics and these metrics should be considered at the synthetic design stage, as some groups already demonstrate. [28, 29] There are multiple routes of degradation for devices, e.g. extrinsic effects and interactions with transport layers, but we focus herein on intrinsic chemical degradation induced by light and oxygen since material resilience to these common stressors is requisite for stable devices. Most design schemes for photostability of OPV materials are based on the generalized but outdated correlations between energy level alignment of polymer electron affinity and ambient reactive species (i.e. molecular oxygen), essentially based on redox properties. For pure OPV polymers, the established mechanisms of photo degradation in light and air consist of radical initiation, propagation, and terminations steps.[30] Initiation occurs via reactive oxygen species that attack the chemical structure, although there are different theories regarding the exact initiation steps and reactive species of photo-oxidation.[1, 31, 32] Conflicting reports propose charge transfer from either a singlet or triplet excited state of the donor to form radical oxygen[33] or the more commonly invoked radical superoxide anion ($O_2^{\bullet -}$), as shown in **Figure 1b**. [1, 32, 34, 35] Based on this construct, one would expect the stability of donor polymers to trend with energy offset to molecular oxygen.

Herein we definitively confirm that a generalization of redox properties alone is insufficient to predict chemical stability of BDTT-based donor polymers. We exposed each of the polymers to accelerated photobleaching in ambient conditions while monitoring the changes to absorption combined with multi time point (and photon dose) spectroscopic chemical analysis. To date, a number of spectroscopic methods have been used to assess degradation mechanisms and determine the products of degradation and site-specific chemical alterations, including X-ray photoelectron spectroscopy (XPS) and infrared (IR) and Raman spectroscopies. [36-42] In this work, we employed XPS for surface-sensitive (5-10 nanometers) detection, with a parts-per-thousand sensitivity to local changes in chemical compositions. This approach ensures that only a few chromophores – namely the ones exposed to the highest oxygen content environment – have been degraded and thus provides early detection of radical propagation and oxygen addition in polymeric materials.

The combination of optical and chemical analysis, combined with literature evidence and precedent, allows us to identify the primary chemical degradation routes, presented as proposed site-specific arrow-pushing pathways. We find that the unique chemical structures of each polymer lead to different relative stabilities that cannot be predicted by the redox properties or prior knowledge of the individual push or pull units. Specifically, we find that monitoring changes in optical density as a function of absorbed photon dose yields decay behavior relevant to the chemical degradation information. We also show that key features of the XPS S 2p and N 1s spectra can elucidate which of the identified chemical degradation pathways are active for each polymer. Overall, our methodology provides a comprehensive example for future studies investigating the relationships between structure and photo-oxidative stability in organic photovoltaic materials. We urge others to measure

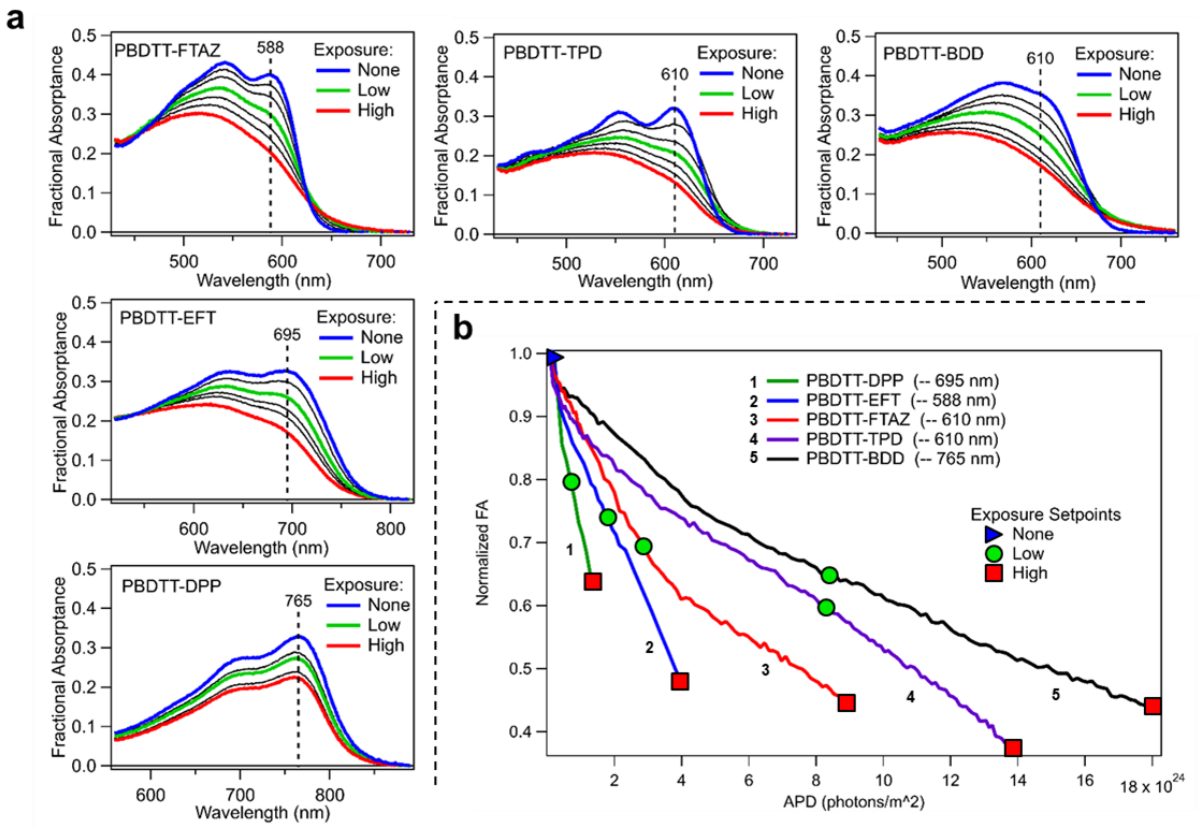

Figure 2. **a)** Primary absorptance features of the five polymers throughout degradation. Dashed lines show the 0-0 wavelength where FA values were extracted for: **b)** the normalized 0-0 transition intensity of each vs. accumulated photon dose (APD). The blue, green, and red traces in **a** and corresponding markers (blue triangle, green circles, red squares) overlaid on each polymer decay in **b** indicate the points at which replicate samples were removed for XPS characterization. The wavelengths of the 0-0 peaks were determined as the center of the lowest-energy peak observed. The exposure information for the none, low, and high setpoints including FA, APD, and time are given in **Table S2**.

photobleaching rates against photon dose (as opposed to change in OD vs time) as a standard practice when first assessing new materials' relative stability. Further, studies should investigate the relationship of decay rates with the material-specific degradation pathways, as demonstrated in this work, in order build a dataset on the structural considerations that are relevant for synthesis of stable materials.

2. Results and Discussion

2.1 Photodegradation and Film Controls.

The photo-generated reactive oxygen mechanism presented in **Figure 1b** accounts for the fact that organic polymers exposed to light without oxygen present, or oxygen without light present, do not undergo rapid photodegradation. Control experiments on the five polymers with peak fractional absorptance (FA) c.a. 0.3-0.4 shown in **Figure S1** confirm that photo-oxidative degradation requires both the presence of oxygen and light. No degradation is observed when only one stressor is applied. Chemical stability was much lower in the case of ambient-light conditions that enable radical formation. Once formed, $O_2^{\bullet-}$ undergoes radical attack of the polymeric structure, which can result in alteration of the chromophore and disruption of the corresponding optical transitions. Fresh unencapsulated polymer films were exposed to a photobleaching lightsource in ambient conditions and absorptance spectra were taken periodically using an automated in-situ photodosing spectrometer (AIPS).[43, 44] Error! Reference source not found.**a** shows the changes to the main absorptance features of each polymer throughout ambient photodosing; all five polymer films exhibit significant photobleaching. **Figure S2** provides the same data set for an expanded wavelength range of c.a. 300-900 nm.

All polymers show reduced absorptance across all wavelengths and none of the polymers show newly arising peaks. PBDTT-DPP decreases absorptance uniformly, with the 0-0 and 0-1 peaks relatively unchanged in position and relative ratio. In contrast, the other 4 polymers exhibit significant peak shifts, broadening, and peak ratio inversions. Thus, the products of degradation are chemical species that are either not optically active in the visible range, have reduced extinction coefficients, or form in small quantities relative to the remaining pristine chromophores. These will be assessed in the next section using x-ray photoelectron spectroscopy.

In **Figure 2a**, we observe that absorptance loss at 0-0 peak wavelengths [18, 25, 45-47] is a consistent feature for each of the five polymers with photo-bleaching. Thus, this polymer-specific wavelength was selected to compare between materials, as it corresponds to the most active chromophores and should

Table 1. Optical density vs APD slopes extracted from linear fits to each of the polymers' absorption decay profiles. Transition points in APD (photons/m^2) determined as the intercept between linear fits as shown in **Figure S4**. A value of OD/APD corresponds to the loss in optical density per photon given the cross section of illuminated film.

Polymer	Decay Wavelength	Initial Decay (OD/APD)	Secondary Decay (OD/APD)	Transition Point (APD)
PBDTT-DPP	765 nm	$-4.15\text{x}10^{-26}$	N/A	N/A
PBDTT-EFT	695 nm	$-2.01\text{x}01^{-26}$	N/A	N/A
PBDTT-FTAZ	588 nm	$-2.31\text{x}10^{-26}$	$-7.52\text{x}10^{-27}$	$3.34\text{x}10^{24}$
PBDTT-BDD	610 nm	$-9.14\text{x}10^{-27}$	$-4.32\text{x}10^{-27}$	$4.95\text{x}10^{24}$
PBDTT-TPD	610 nm	*Nonlinear curvature with inflection point*		$5.87\text{x}10^{24}$

therefore correlate strongly with the chemical changes. Error! Reference source not found.**b** shows a fractional absorptance (FA) line cut at each 0-0 transition peak as a function of accumulated photon dose (APD); wavelengths used are provided in the legend of the graph. The importance of showing optical decay as a function of absorbed photons has been presented previously, including accounting for film thickness variations.[44, 48] Briefly, with photo-bleaching, the polymer films can absorb significantly different photon doses over the same amount of time since each polymer has a unique spectral overlap with the photobleaching lightsource and these profiles change at different rates. Therefore, tracking the reduction of the 0-0 transition relative to APD instead of time is a more rigorous way to assess relative stability.

The rate of absorption decay via photo-oxidation for organic semiconductors is dependent on several variables including microstructure, oxygen concentration, oxygen diffusion coefficients, and the energies and intensities of irradiation. [30, 49, 50] With regard to the optical decay behavior in Error! Reference source not found., a complete and systematic investigation of these variables would be necessary to fully describe degradation kinetics. For example, amorphous microstructures have been shown to photo-oxidize at faster rates for organic semiconductors, attributed to higher oxygen permeability, less conformational rigidity, and/or more localized charges (polarons). [51, 52 53] We performed grazing incidence wide-angle x-ray scattering (GIWAXS) to characterize the packing of the crystalline regions in the 5 polymer films as shown in **Figure S3**. The GIWAXS profiles for the polymers exhibit some ordered scattering but no evidence of long-range order in any of the films, consistent with other reports. [18, 25, 45-47] Thus, we consider the polymers to be in a single comparable phase, as opposed to considering the films two phase systems where different reactivities would be expected.

With this single-phase assumption, we return to the generalization that electron affinity dictates chemical degradation. An observed linear decay in absorption with APD would indicate each absorbed photon causes the same loss to optical density. In other words, each photon of a particular wavelength has the same quantum efficiency for the particular chemical degradation mechanism. Photodegradation pathways involving light of energies not resonant with vibronic transitions in polymers, such as scission or crosslinking, operate over longer time scales and we therefore assume that they do not have significant effects in these experiments. [48, 54, 55] Additionally, the contributions to degradation from residual solvents or impurities are beyond the scope of this work as the focus is on the rapid absorption losses as explained by mechanisms initiated by light and oxygen.

Fits to the linear components of each polymer's decay and identification of the intercept and inflection points, where applicable, are given in **Figure S4** against APD and in **Figure S5** against time. **Error! Reference source not found.** shows the slopes of linear decay and transition points, where relevant, extracted from the fits in **Figure S4**. Linear absorptance losses against APD (Error! Reference source not found.**b**) for PBDTT-DPP and PBDTT-EFT show a strong linear decay correlation for all APD, indicating degradation is likely dominated by a single pathway. Alternatively, PBDTT-FTAZ and PBDTT-BDD exhibit a clear change in slope midway through degradation, suggestive of initial and secondary pathways after a critical photon dose. This relatively distinct switch in decay rates hints at a sequential pair of pathways after a critical uptake of bonded oxygen that corresponds to a saturation of available sites. PBDTT-TPD deviates from linear behavior and has an inflection point where the curvature changes from positive to negative. There may be 3 or more pathways, yet without distinct transitions aside from the inflection point, these could be independently initiated and competing. Concurrent chemical information is needed to investigate these hypotheses.

2.2 Overview of Chemical Degradation Pathways

To investigate the changes in chemical species in the near-surface region, we employed x-ray photoelectron spectroscopy (XPS). Multiples of films were placed on the AIPS system and were removed for analysis after different APDs. This ensured both reproducibility in the measurements and reduced the possibility of the decay rates being affected by experimentation or interruption.

We performed high resolution core-level XPS on the films at three different points in the light-soaking degradation experiment. These points are identified in Error! Reference

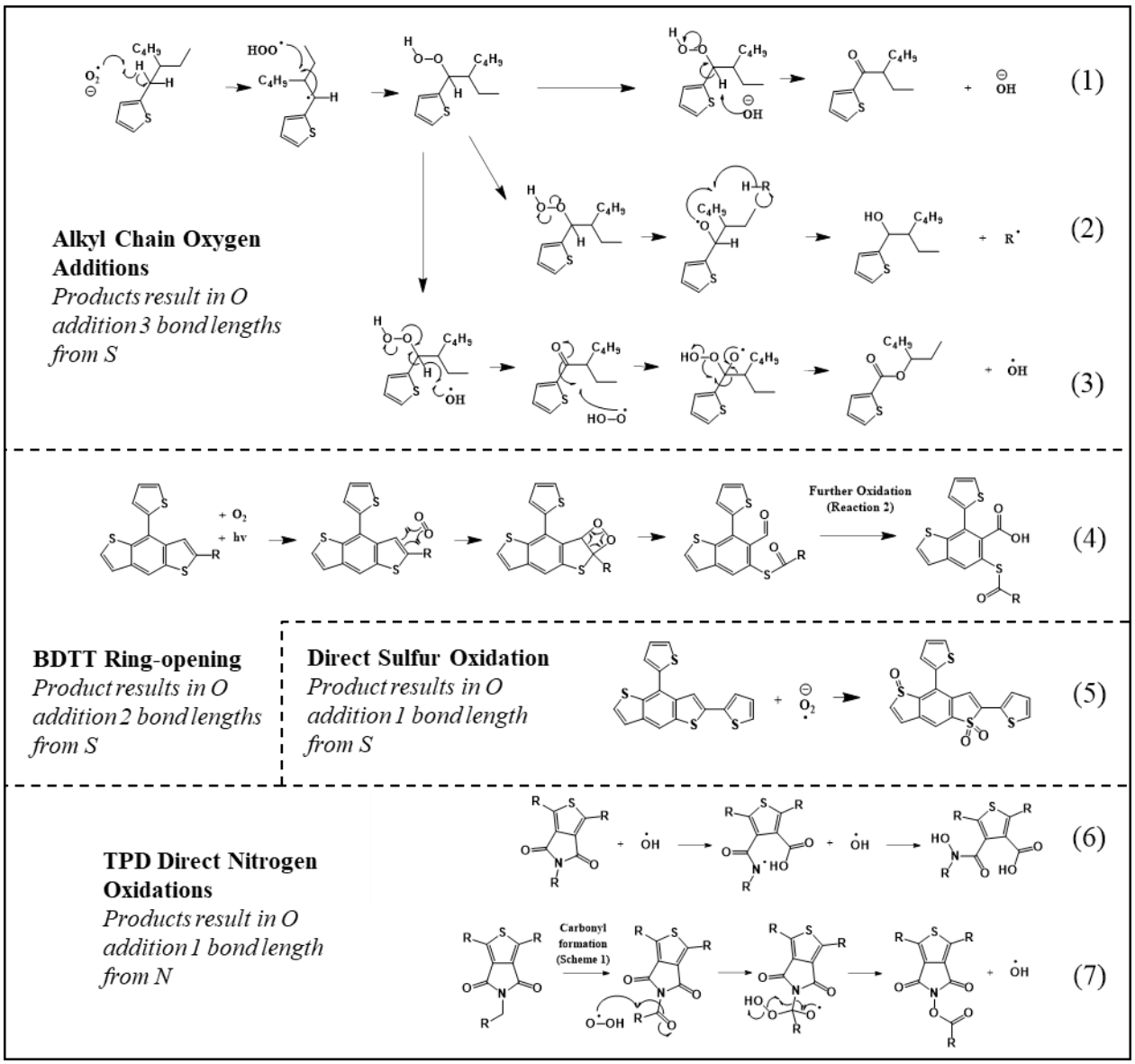

Figure 3. Summary of proposed chemical reactions relevant to the BDTT-based polymers, including oxygen addition on the alkyl chains (reactions 1-3) and the conjugated backbone (reaction 4). Reaction 4 is unique to PBDTT-EFT and proceeds via reaction with molecular oxygen (O_2), consistent with Kim et al.[38] Direct sulfur oxidation, either as a mono- or di-oxidized sulfur atom on thiophene, can occur via reaction 5 while reactions 6-7 are unique to the PBDTT-TPD polymer and result in direct oxidation of the nitrogen of the TPD unit.

source not found. as the exposure levels of "none", "low" and "high"; respectively identified as the blue, green, and red spectra in Error! Reference source not found.**a** and the blue triangle, green circles, and red squares in Error! Reference source not found.**b**. To note, the exposure times and APDs are unique for each polymer since each film was exposed as long as necessary to achieve measurable and distinct absorption loss; greater than c.a. 20% for low exposures and c.a. 35% for high exposures. **Table S2** details the atomic concentrations of each element as determined by XPS for each polymer at each exposure as well as the respective APD, time, and FA. The only significant change to atomic concentrations with exposure is an increase in the oxygen content. The oxygen concentration at the three setpoints for each polymer is plotted against APD in **Figure S6a** and a positive relationship is clear. **Figure S6b** further shows the expected loss in OD as oxygen concentrations increases. This supports the photooxidation mechanism by light exposure in ambient, resulting in chemically bonded oxygen atoms to the polymers structure.

The following sections (*2.3.1-2.3.4*) are case studies for each of the polymers and include the detailed XPS analysis correlated to the optical decay behavior that enabled determinations of the pathways in each of the polymers. In general, the XPS signatures of reporter atoms such as S 2p and N 1s can act as "proximity detectors" to the site of oxygen addition. This allows final products to be identified and pathways to be drawn with consideration of the chemical structures. As an example, supplemental **Note S1** details the process used to correlate S 2p spectral evolution with the formation of specific degradation products.

The results of these case studies are summarized collectively in **Figure 3** as arrow pushing reactions on partial chemical

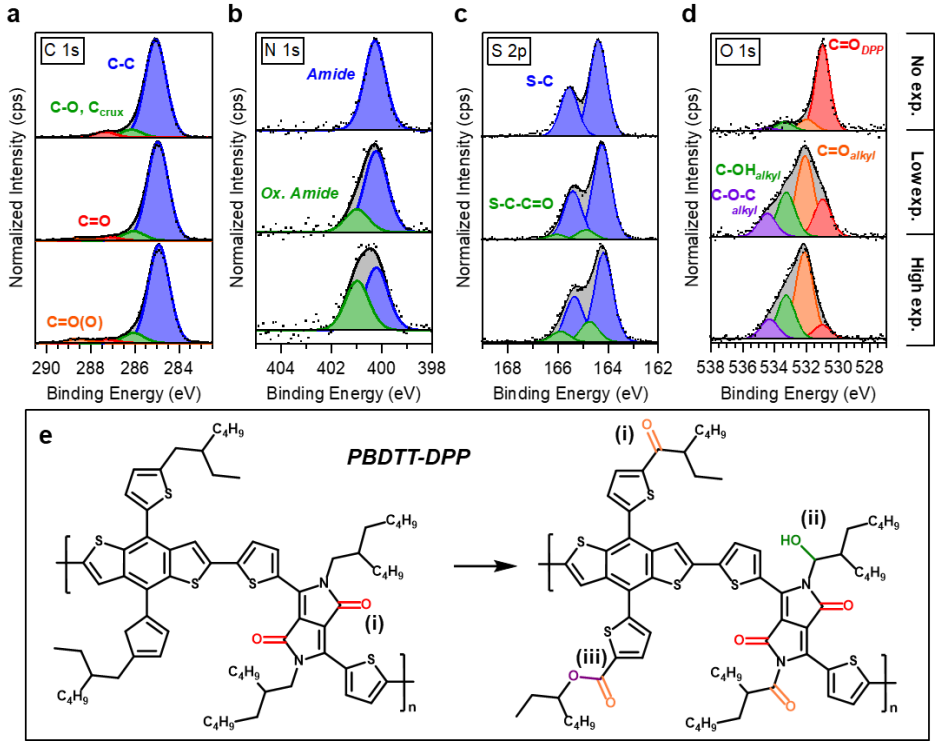

Figure 4. a) C 1s, **b)** N 1s, **c)** S 2p, and **d)** O 1s XPS regional spectra for PBDTT-DPP films with photobleaching exposures of none (top), low (middle), and high (bottom), coinciding with APDs of 0, 7.00E23, 1.37E24, and 2, 4, and 5 average oxygen atoms per monomer, respectively. **e)** The native chemical structure of PBDTT-DPP and proposed structure with superimposed alky-chain oxygen addition products including carbonyls (i), alcohols (ii), and esters (iii), color coded to match O 1s peaks. The degraded structure in **Error! Reference source not found.**e is given to show the possibilities for degradation products superimposed on the same monomer for brevity.

structures to be relevant for all the polymers. Supplemental **Note S2** includes further details on the exact steps and literature support for each reaction. In **Figure 3**, reactions are grouped by indistinguishable final products, i.e., those that have the same reporter atom signatures in XPS, including oxygen addition on the alkyl chains (**reactions 1-3**) and the conjugated backbone (**reaction 4**). We readily acknowledge that we cannot confidently discriminate between the pathways and products of **reactions 1-3** but have included all pathways where the first C-H bond of side chains are attacked by oxygen to form carbonyls, alcohols, or esters. The ring-opening **reaction 4** was proposed by Kim et al. for PBDTT-EFT [42] and occurs on the conjugated backbone of BDTT via a charge transfer state and results in formation of a thioester and carboxylic acid. Direct sulfur oxidation, either as a mono- or di-oxidized sulfur atom on thiophene, can occur via **reaction 5** while **reactions 6-7** are unique to the PBDTT-TPD polymer and result in direct oxidation of the nitrogen of the TPD unit.

2.3 Case Examples for Degradation

2.3.1. Case Example I: Alkyl Chain Oxygen Addition in PBDTT-DPP

The PBDTT-DPP polymer provides an effective case study for photodegradation by alkyl chain oxidation pathways. Error! Reference source not found.**a-d** shows the XPS regional spectra for PBDTT-DPP films after none, low, and high photon dose exposures; the order of the panels (top to bottom) corresponds to increasing exposure time. The corresponding fit parameters including chemical assignment, peak position, full-width half-max, and area percentage are given in **Table S3**.

A detailed analysis correlating the XPS signatures with photodegradation species is given in supplementary **Note S3**. To summarize, in the C 1s spectra in Error! Reference source not found.**a**, we observe an increase in the relative contributions of the higher BE peaks (green, red, orange). We assign these peaks to the formation of alcohols (C-O), carbonyls (C=O), and esters (C=O(O)), respectively. [36, 41, 52, 56] The N 1s spectra in Error! Reference source not found.**b** for the pristine film has a single peak at approximately 400.3 eV associated with the amide group of the pull unit. A shoulder emerges with even low photon dosing (14% bleach), this develops to the higher BE component (green) shifted c.a. 0.7 eV relative to the amide to c.a. 401.0 eV. This BE shift is consistent with a hemi-aminal, or oxidation of the carbon atom adjacent to the amide nitrogen, and not direct oxidation of the nitrogen atom itself which has been shown to result in a larger BE shift (c.a. 2 eV). [44, 57, 58] Alternatively, in our data the DPP skeleton remains intact but an alkyl chain oxygen addition is hypothesized to occur on the side chains of the DPP unit. The S 2p doublet spectra are provided in **Figure 4c**. With no accumulated photon dose, we readily observe the expected spin-orbit coupling of the two peaks with a ratio of 2:1 for the S2p$_{3/2}$ to S2p$_{1/2}$, respectively. With both low and high photon dosing, we observe the formation of a second doublet (green) approximately 0.6 eV from the native thiophene sulfur peaks (blue). This shift is

consistent with a perturbation to a branching thiophene's sulfur atom by added oxygen 3 bond lengths away (on the alkyl chain) based on the reporter atom analysis in **Note S2**. Notably, there is no evidence of thioesters or directly oxidized sulfur species. The O 1s spectra in Error! Reference source not found.**d** are consistent with **reactions 1-3** exhibiting formation of carbonyls, alcohols, and esters. We can conclude that these products form on the alkyl chains of both the push and pull units from proximity to the nitrogen and sulfur reporter atoms, respectively.

Additionally, PBDTT-DPP also exhibited the most rapid increase in bonded oxygen with respect to APD (**Figure S6a**), likely due to availability of initiation sites (4 alkyl chains per monomer). The lack of degradation pathways directly affecting the chromophore is consistent with minimally impacted bandgaps and corresponding absorption features, though it may be that chromophore alterations are occurring that result in chemical shifts below the sensitivity of XPS. We readily acknowledge additional factors may impact the magnitude of optical density loss; the loss of 32% in the case of PBDTT-DPP

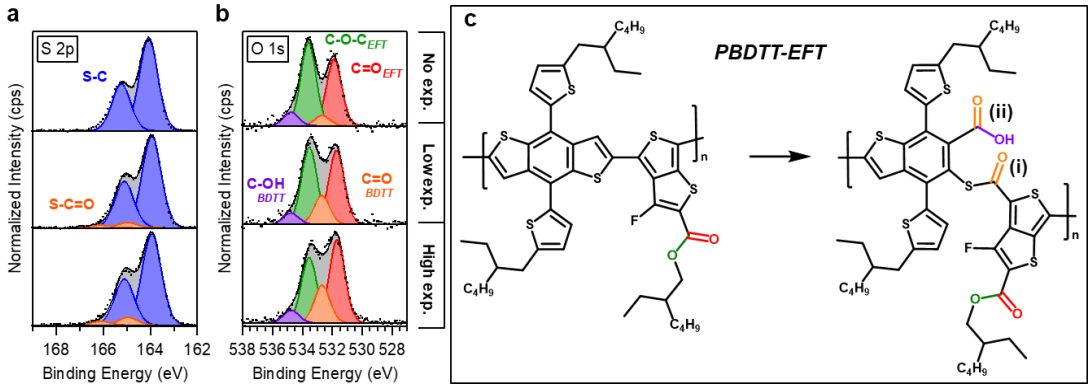

Figure 5. a) S 2p and **b)** O 1s XPS regional spectra for PBDTT-EFT films with photobleaching exposures of none (top), low (middle), and high (bottom), coinciding with APDs of 0, 1.84E24, and 4.04E24 and 2, 3, and 4 average oxygen atoms per monomer, respectively. **c)** The native chemical structure of PBDTT-EFT and a suggested structure following the **reaction 4** pathway with thioester (i) and carboxylic acid (ii) formation; color coded to match O 1s peaks.

Connecting the XPS data described above to the OD decay of PBDTT-DPP discussed in **section 2.2** and Error! Reference source not found. further corroborates a single dominant degradation mechanism or set of reactions. The native chemical structure of PBDTT-DPP and an example degraded structure following alkyl chain oxygen addition at the determined sites are shown in Error! Reference source not found.**e**; we don't anticipate that all degraded products would appear on the same monomer unit necessarily. The degraded structure in Error! Reference source not found.**e** is given to show the possibilities for degradation products superimposed on the same monomer. The average number of oxygen atoms per monomer (**Table S2**) increased from 2 (native) to 5 (high exposure), although this quantification is only valid within the sampling depth of XPS (5-10 nm). There is likely some fraction of the monomer units that has undergone significant oxidation as shown in Error! Reference source not found., just as there is likely some fraction that remains unaltered, and other fractions with varying degrees of oxidation. It is beyond the scope of this study to determine these fractions. However, if we assume that only the top 8 nm of the film is affected, a film density of 1.5 g/cm^3 and spot size of 300 um^2, then there are approximately 1.7 x 10^{11} affected monomers. The collective effect of these alkyl chain oxidations reduced the bulk film optical density by 32% for the highly exposed sample. This might be surprising given the lack of alterations affecting the conjugated backbone, but the absorption profile of PBDTT-DPP shown in Error! Reference source not found.**a** exhibited little change to the profile *shape* relative to the other polymers.

may be due to a combination of disrupted chromophore functionality and possibly light-only or thermally induced alterations such as crosslinking or scission that are not detectable via XPS.

To summarize, the degradation behavior of PBDTT-DPP was dominated by alkyl chain oxygen addition occurring at the alpha carbon of side chains on both the push and pull units. PBDTT-DPP also had the greatest increase in bonded oxygen with respect to APD of the polymers and the most rapid decay in optical density with respect to both APD and time. The latter point is surprising given the lack of degradation mechanisms affecting the conjugated backbone. The absorption intensity of a PBDTT-DPP film may therefore be highly dependent on the microstructure or chemical changes that cannot be detected via XPS, consistent with the absorption changes observed for control films in the dark in air and in the light in an inert environment.

2.3.2 Case Example II: BDTT Ring-opening in PBDTT-EFT

We look next to a ring-opening mechanism on the BDTT unit responsible for the degradation of PBDTT-EFT (aka PTB7-Th or PCE10). This pathway was previously proposed by Kim et al. based on absorption, photoluminescence, and Raman analysis, [42] which provides a relevant benchmark for the sensitivity of our XPS approach. Error! Reference source not found.**a-b** shows selected XPS regional spectra for PBDTT-EFT films after none, low, and high photon dose exposures; the order of the panels (top to bottom) corresponds to increasing exposure time. The corresponding fit parameters including chemical assignment, peak position, full-width half-max, and area percentage are

given in **Table S4**. Supplemental **Note S4** provides the C 1s and F 1s core levels, with C 1s exhibiting a clear increase in higher BE species with ambient photodosing (as shown for PBDTT-DPP) while the F 1s spectra is unaffected.

In **Figure 5a**, the S 2p doublet again yields a new species of sulfur (orange) that arises with exposure shifted from the native thiophene (blue) by c.a. 1.0 eV. This is consistent with oxidation of the thiophene ring carbon bonds. We note this relative binding energy shift is in between the 0.6 eV shift of S 2p peaks observed for BDTT unit alkyl chain oxygen addition and the larger shift (c.a. 4 eV) expected for direct sulfur oxidation (i.e. sulfoxide and/or sulphonyl formation). We also note that the EFT alkyl chain already has a native ester to protect that site for **reactions 1-3**, although oxygen addition to a non-alpha carbon on the alkyl chain could be possible. The O 1s spectra in Error! Reference source not found.**b** show that the peaks assigned to thioester and carboxylic acid oxygen atoms formed on the BDTT push unit (orange and purple) increase with exposure relative to the native ester oxygen atoms (red and green) on the EFT pull unit. Error! Reference source not found. shows the native chemical structure of PBDTT-EFT and an example of a degraded structure that follows **reaction 4** with a BDTT ring-opening mechanism. We note from **Table S2** that the average number of oxygen atoms per monomer on the surface of the film has increased from 2 (native) to 4 (high exposure) though we again expect an unequal distribution across monomers in the film.

Collectively, our results are in agreement with Kim et al. that the dominating degradation pathway is **reaction 4**: thioester and carboxylic acid formation via ring opening at the benzo-adjacent thiophene of the BDTT unit. As shown in **reaction 4**, the initiation of this pathway is assumed to be via a charge transfer state between the polymer and molecular oxygen (O_2), rather than reacting with a radical oxygen species. We note that the behavior of PBDTT-EFT is very different from that of PBDTT-DPP, despite the two having almost equivalent electron affinities shown in **Figure 1b**. The result for PBDTT-EFT is a reaction that is highly site-localized to the conjugated system where the photoelectron is highly distributed. Therefore, it is consistent that a material dominated by this process does not also significantly undergo any of the other degradation pathways since they all require a reactive species to migrate to initiation sites. This is also in agreement with Löhrer et al. who identified the most sensitive reaction site of the polymer to be the conjugated backbone.[48]

A single dominating degradation pathway is also corroborated by the sole linear decay to optical density for PBDTT-EFT as discussed in **section 2.2** and Error! Reference source not found.. This polymer provides a second interesting comparison to PBDTT-DPP since they both have singular pathways and linear optical decays. However, PBDTT-EFT displays greater change to the absorption profile as a whole including peak broadening, a declining 0-0 to 0-1 ratio, and a blueshift to the onset (Error! Reference source not found.**a**). The thiophene ring-opening pathway dominant in PBDTT-EFT is responsible for the loss in optical density through direct disruption of the chromophore. These disruptions to the conjugated backbone of the polymer could also explain why PBDTT-EFT, in contrast to PBDTT-DPP, exhibited not only optical density losses but an evolving absorption profile. Further, this would explain why PBDTT-EFT had the most rapid decay in optical density with respect to added oxygen concentration in **Figure S6b**: added oxygen has a significant impact on the chromophore of the polymer. As there are only 2 sites per monomer for this pathway to occur, this mechanism is expected to be relatively slow. In contrast the alkyl chain oxygen addition mechanism proposed for PBDTT-DPP has a less direct effect on the chromophore and but there are 4 sites for initiation per monomer.

Overall, despite being one of the more commonly used polymers in current research, PBDTT-EFT was the second most unstable polymer in the study and its degradation was dominated by a ring-opening mechanism on the BDTT backbone. This mechanism was unique in that it only occurred for PBDTT-EFT and it is proposed to be initiated via a charge transfer state between the polymer and molecular oxygen, as opposed to creation of a radical species. We postulate that since PBDTT-EFT had the smallest bandgap and therefore the smallest push-pull effect, the energetic driving force for charge separation was not sufficient to fully transfer photo-excited electrons to oxygen. One possible counterintuitive consequence for chemical design is that improving the ability of a polymer to transfer electrons to oxygen may reduce the rate of degradation as the reactive species could then migrate to other sites such as the alkyl chains as opposed to directly affecting the chromophore, suggesting potential upside for revisiting the design of wide-gap donor polymers with preferentially sacrificial side chains and protected backbones. The implication for the stability of OPV active layers is that an acceptor material could not compete as effectively with oxygen for electron harvesting if oxygen can diffuse to closer proximity and react with the polymer via a rapid transfer state. Future studies could investigate if the radical scavenging effect of acceptors is less effective in lower bandgap polymers. We now look to the remaining three polymers, which all show evidence of multiple active degradation mechanisms.

2.3.3 Case Example III: Direct Sulfur Oxidation in PBDTT-FTAZ & PBDTT-BDD

We now turn to the polymers PBDTT-FTAZ and PBDTT-BDD which both show evidence of a sequential pair of degradation pathways in **Figure 2b**. PBDTT-BDD, also called PBDB-T, is the parent compound for a family of derivatives including PM6 that have enabled device efficiencies over 19%.[9, 26, 27] The chemical structure only consists of carbon, sulfur, and oxygen. The lack of reporter atoms makes localizing degradation pathways difficult but the similarity of the absorption decay characteristics (Error! Reference source not found.**b** and **Figure S4**) and residual S 2p spectra (**Figure S7**) to PBDTT-FTAZ, which does carry a variety of reporter atoms, indicates similar degradation pathways.

Figure a and **Figure 6c** show the S 2p XPS regional spectra for PBDTT-FTAZ and PBDTT-BDD films, respectively, after none, low, and high photon dose exposures; the order of the panels in **Figures 6a** and **Figure 6c** (top to bottom) corresponds to

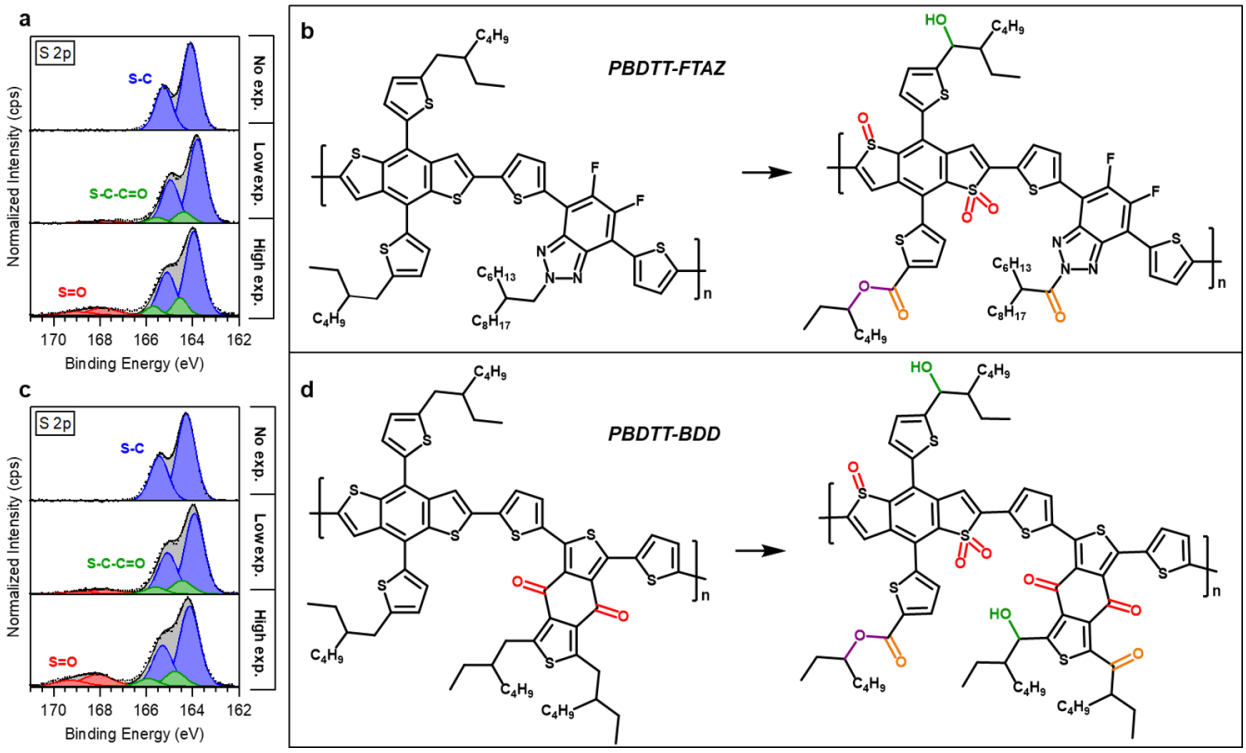

Figure 6. S 2p XPS regional spectra for PBDTT-FTAZ **(a)** and PBDTT-BDD **(c)** films with photobleaching exposures of none (top), low (middle), and high (bottom). PBDTT-FTAZ exposures correspond to APDs of 0, 2.88E24, and 9.00E24 and 0, 4, and 8 oxygen atoms per monomer, respectively. PBDTT-BDD exposures correspond to APDs of 0, 8.35E24, and 1.82E25 and 2, 8, and 17 oxygen atoms per monomer, respectively. The native chemical structures of **b)** PBDTT-FTAZ and **d)** PBDTT-BDD with a proposed degraded structure following alky-chain oxygen addition and direct sulfur oxidation. Note that all functional groups may not occur on one monomer unit but are shown here to summarize. Oxygen species color coded to match O 1s peaks in SI.

increasing exposure time. The corresponding fit parameters including chemical assignment, peak position, full-width half-max, and area percentage are given in **Table S5** and **Table S6**. The S 2p spectra for both polymers show the arrival and increase of two distinct spin-orbit coupled peak pairs with exposure: one shifted c.a. 0.6 eV (green) and one c.a. 4.0 eV (red) from the native thiophene peaks (blue). The peaks shifted c.a. 0.6 eV were previously observed for PBDTT-DPP (and delineated in **Note S2**) and correspond to products of alkyl chain oxidation. The peaks shifted by c.a. 4.0 eV correspond to directly oxidized sulfur, as previously observed in other thiophene-containing polymers including P3HT,[38, 59 41, 60] PTB7, [56] PDPP4T, [44] and PCPDTBT. [40] Detailed analysis with the excluded regional spectra correlating the XPS signatures with photodegradation species are given in **Note S5** for PBDTT-FTAZ and **Note S6** for PBDTT-BDD. In summary for both polymers, the C 1s and O 1s spectra show the expected increase in peaks that correspond to formation of alcohols, carbonyls, and esters. PBDTT-FTAZ also contains fluorine, which is unaffected per the F 1s spectra (**Figure S10b**), and nitrogen. The N 1s in **Figure S10c** shows a new peak that we assign to an oxidized triazole, or an oxidation of a carbon atom adjacent to the triazole (see **Note S5** for rationale).

The C 1s, O 1s, and S 2p spectra all indicate that **reactions 1-3** are active in both PBDTT-FTAZ and PBDTT-BDD resulting in alkyl chain oxygen addition. For PBDTT-BDD, the reporter atoms (sulfur) for the alkyl chains alpha carbons on the push and pull units are spectroscopically identical. Thus, we cannot determine if alkyl chain oxidation is occurring on one unit or both. For PBDTT-FTAZ however, the sulfur reporter atoms in **Figure 6a** suggest that oxygen addition is occurring at the alpha carbon site on the BDTT unit while the nitrogen reporter atom does the same for the FTAZ unit. Thus, alkyl chain oxygen addition is occurring on both structural units of PBDTT-FTAZ. The S 2p spectra additionally indicate direct sulfur oxidation is prevalent in both polymers following **reaction 5**. The products could be either a mono- or di-oxidized sulfur atom. [61-63] The S-O products are more likely to occur on thiophenes that are a part of a larger conjugated system, such as benzodithiophene, than those that are more isolated due to lower energy barriers.[61] Combining these results, **Figure 6b** and **Figure 6d** show the native chemical structures of the two polymers as well as likely degraded structures using superimposed products of alkyl chain oxygen addition and sulfur oxidation.

The relationship (concurrent vs sequential) and relative impact of the active degradation pathways is of interest when there are multiple reactions occurring. As discussed in **section 2.2** and shown in Error! Reference source not found., the optical decay vs APD for both PBDTT-FTAZ and PBDTT-BDD indicate two sequential degradation pathways, potentially after a critical photon dose point. Analysis of the S 2p peak areas in **Figure 6a** and **Figure 6c** (**Table S5** and **Table S6**) reveal that the peaks corresponding to alkyl chain oxidation products (green) primarily increase in relative area during the initial linear optical

decay while those of sulfur oxidation products are negligible. The alkyl chain oxidation products appear to stop forming in significant amounts while the sulfur oxidation products relatively increase. This is readily apparent in **Figure a** and **Figure 6c** as the green peaks have formed by the low exposure point (middle panel) while the red are minimal. Then by the high exposure point (bottom panel) the green peaks are minimally larger in area but the red peaks have grown substantially. We find (details in **Notes S5** and **Note S6**) that the change in dominant product formation occurs at approximately the same APD as the critical point in OD rates in Error! Reference source not found.. Thus, we can assign the initial OD decay of PBDTT-FTAZ and PBDTT-BDD films to degradation by **reactions 1-3** and the secondary decay to **reaction 5**.

The sulfur oxidation pathway in PBDTT-FTAZ required c.a. 3 times the APD of alkyl chain oxygen addition to result in the same absorption loss. The average number of oxygen atoms per monomer (**Table S2**) went from 0 (native) to 4 (low exposure) to 8 (high), and the switch in optical decay slopes occurred at an APD close to the low exposure point. Thus, 4 average oxygen atoms per monomer at the low exposure point, sufficient to saturate the 3 available alkyl chain initiation sites per PBDTT-FTAZ monomer, coincides with the switch in mechanisms. This indicates that the initial degradation was dominated by alkyl chain oxygen addition but when the available sites were saturated, sulfur oxidation proceeded without competition.

The sulfur oxidation pathway in PBDTT-BDD required c.a. 2 times the APD of alkyl chain oxygen addition to result in the same absorption loss. The average number of oxygen atoms per monomer for PBDTT-BDD (**Table S2**) increases from 2 (native) to 8 (low exposure) to 17 (high). This is a much larger uptake in bonded oxygen than observed for the other polymers, consistent with PBDTT-BDD having the greatest resilience to absorption decay with increasing oxygen concentration as observed in **Figure S6b**. The film still retained 49% of its optical density by the high exposure point despite an extra 15 average oxygen atoms per monomer. As the low exposure point (8 average oxygen atoms per monomer) is at an APD higher than the switching photon dose, we extrapolate the average oxygen atoms per monomer to the switching dose to find it coincides with 6 average oxygen atoms per monomer, the exact number of alkyl chain initiation sites (alpha carbons), substantiating the saturation of alkyl chain oxygen addition. Due to the high oxygen uptake of PBDTT-BDD relative to the others in the study, there are likely further oxidation pathways occurring beyond those shown in **Figure d**. The most likely site for continued oxidation is along the alkyl chains, however, after oxygen attachment at the first (alpha) site, further oxidation along the chains is less likely to have significant effects on absorption. We therefore expect the second linear decay to absorption to be primarily due to sulfur oxidation with the possibility of non-trivial contribution from continued alkyl chain oxidation.

In summary, the PBDTT-BDD (PBDB-T) and PBDTT-FTAZ polymers exhibited similar degradation behavior with an initial fast OD decay due to alkyl chain oxygen addition then a switch in mechanisms to direct sulfur oxidation of backbone thiophene and a slower OD decay. For these polymers, the sulfur oxidation mechanism requires 2-3 times the APD as alkyl chain oxidation to result in the same OD loss. This likely indicates that an absorbed photon has a lower probably of resulting in sulfur oxidation, especially when preferential side chain attack sites are available. Despite similar degradation pathways, PBDTT-BDD was the most stable polymer of the 5 in the study while PBDTT-FTAZ was in the middle. This was primarily due to the greater initial optical decay from alkyl chain oxidation in PBDTT-FTAZ, as the slopes of decay during sulfur oxidation were comparable. Overall, PBDTT-FTAZ had both a greater probability of an absorbed photon resulting in bonded oxygen and a greater reduction in absorption per oxygen atom added. The probability of bonded oxygen resulting in a loss of optical density was the lowest for PBDTT-BDD of all the polymers.

2.3.4 Case Example IV: Direct Nitrogen Oxidation in PBDTT-TPD

We now turn to the final polymer, PBDTT-TPD, which of the polymer set has unique absorption decay characteristics and a new degradation pathway. Error! Reference source not found.**7a-d** show all the XPS regional spectra for PBDTT-TPD films after none, low, and high exposures to ambient photodosing; the order of the panels (top to bottom) corresponds to increasing exposure time. The corresponding fit parameters including chemical assignment, peak position, full-width half-max, and area percentage are given in **Table S7**. A detailed analysis correlating the XPS signatures with photodegradation species is given in **Note S7**. To summarize, the C 1s spectra in Error! Reference source not found.**a** shows the expected increase in higher BE species (C-O, C=O, C=O(O)) with exposure. The blue peak in the N 1s spectra in Error! Reference source not found.**b** corresponds to the nitrogen in the pyrrole dione of the TPD unit. Upon exposure, we observe new species shifted to higher BE by c.a. 1.0 eV (green) by c.a. 2.0 eV (orange). We assign the former to an oxidized pyrrole dione, whereby the alpha carbon of adjacent alkyl chain has been oxidized and the latter peak to directly oxidized nitrogen.[44] The oxidized pyrrole dione case is denoted in Error! Reference source not found.**e** as (i) and the oxidized nitrogen case as (ii). The S 2p spectra in Error! Reference source not found.**c** show similar trends as observed for the BDD and FTAZ pull systems indicating direct sulfur oxidation. There is a significant increase in the (green) spin-orbit coupled peak pair shifted c.a. 0.6 eV from native thiophene (blue) by the low exposure point but a minimal increase from the low to the high exposure points. The red peaks shifted c.a. 4.0 eV from native thiophene have minimal presence by the low exposure point but increase significantly between the low and high exposure points.

Together, the C 1s, N 1s, and S 2p spectra indicate the formation of alkyl chain oxidation and sulfur oxidation products, as was in the case of PBDTT-FTAZ, via **reactions 1-3** and **reaction 5**, respectively. The alkyl chain oxygen addition occurs on both the push and pull units as evidenced by the oxidized pyrrole dione peak (green) in the N 1s and the S-C-C=O peak (green) in the S 2p. The directly oxidized sulfur evidenced by the S-O peak (red) in the S 2p spectra is again assumed to occur on conjugated backbone thiophene. Interestingly, the peak

assigned to directly oxidized nitrogen (orange) the N 1s spectra suggests a third pathway in PBDTT-TPD. Oxidized nitrogen necessitates a pathway where the pyrrole dione is opened to allow the formation of an N-O bond. We determine this to most likely be via the **reaction 6** pathway as discussed in detail in **Note S7**. Since nitrogen species of both oxidized pyrrole diones and directly oxidized nitrogen are present by the low exposure point, it is not clear if the direct nitrogen oxidation pathway initiates independently as in **reaction 6** or proceeds from an alkyl chain oxygen addition as in **reaction 7**. The average number of oxygen atoms per monomer increased from 2 (native) to 5 (low exposure) to 9 (high) (**Table S2**) and we note a 59% loss to optical density by the high exposure point. Error! Reference source not found.**e** shows the show the native chemical structure of PBDTT-TPD as well as a likely degraded structure using superimposed products of alkyl chain oxygen addition, sulfur oxidation, and pyrrole dione ring-opening.

found.**c** once again indicate competition between alkyl chain oxidation and sulfur oxidation where the latter proceeds after saturation of the former. There was no linear slope change to the 0-0 transition decay in **Figure S4** that could be associated with the saturation of alkyl chain initiation sites, but extrapolation of the data in **Table S2** to the APD of the curvature change identified previously yields 4 average oxygen atoms per monomer, which corroborates saturation of the 3 available initiation sites. This point also occurs at lower APD than the low exposure point, at which we observe a small contribution of oxidized sulfur products (**Table S7**). The change in curvature at this point is thereby likely due to the termination of alkyl chain oxygen addition and the onset of direct sulfur oxidation. Notably, XPS results indicate that the pyrrole ring-opening pathway is active throughout the full photobleaching experiment. Thus, the two regions of distinct curvature in PBDTT-TPD absorption decay (Error! Reference source not

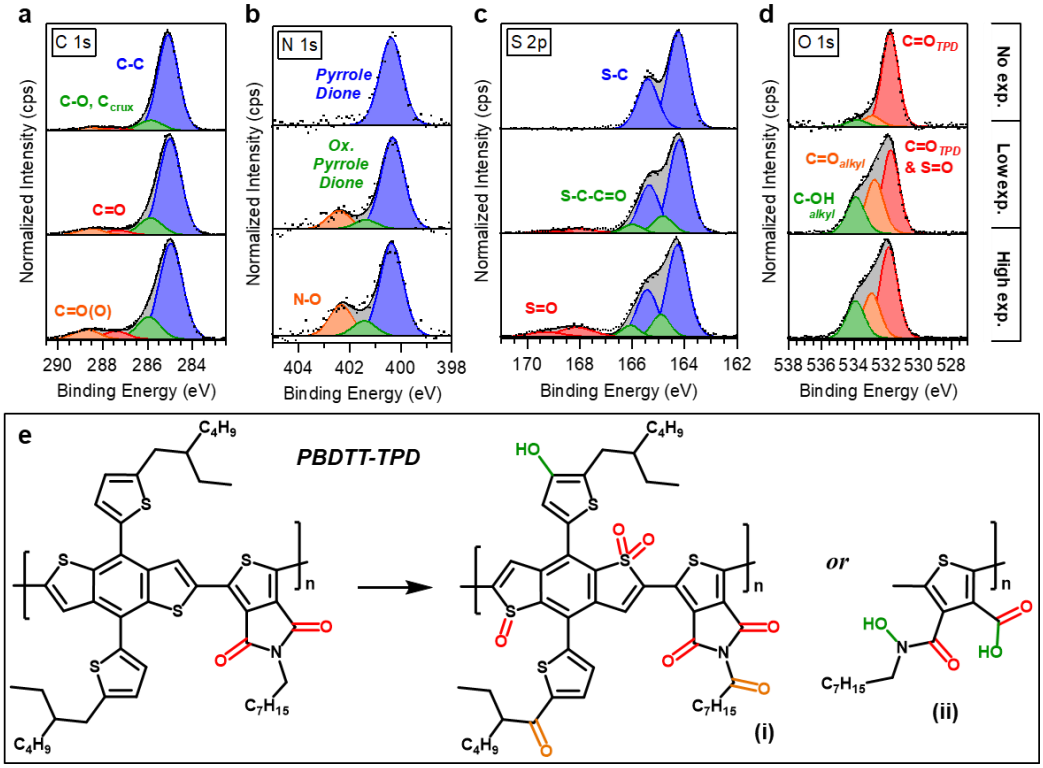

Figure 7. a) C 1s, **b)** N 1s, **c)** S 2p, and **d)** O 1s XPS regional spectra for PBDTT-TPD films with photobleaching exposures of none (top), low (middle), and high (bottom), coinciding with APDs of 0, 8.28E24, and 1.40E25 and 2, 5, and 9 average oxygen atoms per monomer, respectively. **e)** The native chemical structure of PBDTT-TPD and examples of possible degraded structures with superimposed products of (i) alkyl chain oxygen attack and direct sulfur oxidation, and (ii) pyrrole dione ring-opening; oxygen species color coded to match O 1s peaks.

From **Figure 2b**, the 0-0 optical transition decay of PBDTT-TPD discussed in **section 2.2** did not exhibit clear linear regions. We attribute this to the competition of the 3 different sets of degradation pathways where the combination of multiple rates and transition points result in nonlinear behavior. As fitting the decay to a polynomial function removes physical relevance of the coefficients, we sufficed to identify the change in curvature to be at 5.87x1024 APD (Error! Reference source not found.**Error! Reference source not found.**), determined as the change in sign of the second derivative in **Figure S4**. The peak growth characteristics in the S 2p in Error! Reference source not found.**b**) are likely each the combination of two degradation pathways. The initial optical density decay (positive curvature) being due to alkyl chain oxygen addition and pyrrole ring opening, and the subsequent behavior (negative curvature) is the result of pyrrole ring opening and sulfur oxidation.

We note that PBDTT-TPD was the only polymer that showed strong evidence of 3 different degradation pathways and the competition between them likely resulted in the relative stability of the material (second most stable). Similar to PBDTT-BDD and PBDTT-FTAZ, the alkyl chain oxygen addition mechanism eventually saturated and sulfur oxidation then

proceeded. However, the third mechanism of pyrrole ring opening was active throughout the photodegradation experiment. We previously rationalized that a single dominating pathway is expected due to competition for the reactive species. For this reason, sulfur oxidation is not prevalent in any polymer until alkyl chain oxidation is saturated: they both initiate with the radical superoxide anion ($O_2^{\bullet -}$) and the alpha carbon of side chains was more energetically favorable for reaction than a thiophene sulfur atom. The pyrrole ring-opening pathway for PBDTT-TPD, however, does not initiate with the same radical species and could therefore proceed simultaneously.

2.4 All Polymer Comparison Summary

We highlight that the relative stability between all 5 polymers did not form a robust trend with electron affinity (EA). That is, the probability of an absorbed photon to result in a loss in optical density does not appear to be a function of the driving force between the polymer S_1 or T_1 states and EA of molecular oxygen. The overall absorption decay of the polymers was dependent on the unique chemical structures. When considering the full polymer set, it is clear that if redox levels are sufficient to initiate photooxidation, stability then depends highly on the specific degradation pathway(s) as to whether photooxidation primarily attacks the side chains or backbone, which impact the chromophore and optoelectronic properties of the polymer differently.

If, however, we isolate degradation solely attributed to alkyl chain oxygen attack (case example I and the initial decay regions in case example III), we observe a trend of faster decay with higher polymer EA. In other words, the degradation rate via **reactions 1-3** was highest for PBDTT-DPP (EA=3.63 eV), median for PBDTT-FTAZ (EA=3.24 eV), and lowest for PBDTT-BDD (EA=2.92 eV). For this subset, there is also a trend of higher oxygen uptake per absorbed photon with polymer EA. Similarly, the trend holds true when isolating degradation solely due to direct sulfur oxidation (secondary decays in case study III). These constrained results indicate that when kinetics don't outcompete thermodynamics (i.e. considering a single degradation pathway on nearly identical structural sites), the redox properties are then dominant for degradation probability.

These constrained results would indicate that for BDTT-based polymers undergoing the same chemical reaction pathways, a higher EA means greater susceptibility to photobleaching. However, assuming an EA of 3.75 eV for molecular oxygen,[1] which is higher than any of the polymers, we find it more likely that photobleaching susceptibility increases as polymer EA approaches oxygen EA. This would indicate that electron transfer from an excited polymer to molecular oxygen is facilitated by the degree of energetic coupling between the respective states. That is, if $EA_{O2} > EA_{polymer}$, then the probability of photooxidation increases as $EA_{O2} - EA_{polymer}$ approaches 0.

Regardless of these trends that exist within specific decay regions of a limited set of the BDTT-based polymers, overall photostability was primarily dependent on the unique chemical structures and specific degradation pathways. Comprehensive chemical-stability studies like this can aid the development of stable materials with actionable synthetic guidelines far beyond the simple, and non-universal, correlations of electron affinity with light-air stability. Knowledge on the relationship between optical decay and material-specific degradation pathways will build a dataset on the structural considerations that are relevant for development of stable materials. At the very least, measurement of photobleaching rates as a function of APD should become standard practice as a first assessment of new materials' relative stability.

4. Conclusions

We have shown that knowledge of the redox properties or stability of the individual components is not sufficient to predict the stability of push-pull polymers. Rather, each chemical structure must be evaluated as a complete construction since the full structure influences the location of primary attack sites, the competition between and types of degradation pathways, and the final products – the sum of which determines material performance durability. Even when the same chemical degradation pathways are active in different polymers, they demonstrate different absorption tolerances to the alterations depending on whether their chemical designs favor oxygen attack at side chain vs backbone. We found that alkyl chain oxygen addition and sulfur oxidation were prevalent degradation pathways, and that the latter generally initiates after saturation of the former. These results applicable for organic semiconductors beyond push-pull polymer architectures, particularly since most share the basic structural template of alkyl chains on a conjugated backbone. Our findings should motivate new side-chain chemical design functionalities that go beyond solubility and microstructure formation assistance, to also aid in sacrificial reactive oxygen scavenging since side chain attack is less detrimental to optoelectronics and can outcompete rates of backbone attack. This work also showcased the ability XPS to elucidate final products and attack sites of chemical degradation through detailed, self-consistent, and comprehensive analysis of the regional spectra. Reporter atoms such as sulfur and nitrogen yielded valuable information in this regard. It is apparent in this work that the pull components of BDTT-push polymers influence the relative stability and mechanisms of ambient photo-induced chemical degradation primarily as they form chemical arrangements with unique susceptibilities. The conclusions and characteristics observed can be applied to the optimization of current or future OPV materials.

5. Experimental

5.1 Materials and Sample Preparation.

PBDTT-BDD (PBDB-T) was purchased from Brilliant Matters, PBDTT-FTAZ (J52) was purchased from Lumtec, PBDTT-DPP and PBDTT-TPD were purchased from Ossila, and PBDTT-EFT (PCE10) was purchased from 1-Material. Polymer films were all

cast from chloroform solutions at 4 mg/mL, except for PBDTT-DPP which was 2 mg/mL, to achieve films with maximum optical densities c.a. 0.4. Solutions were heated on a hotplate at 45 ˚C prior to spincoating in an inert N2 glovebox with the following recipe: (1000 rpm for 1 s)-(800 rpm for 45 s)-(1000 rpm for 1 s) using approximately 90-110 uL of unfiltered solution per cast. Samples were kept in dark N2 environments for storage and transport and were only exposed to air during degradation testing. Chemical structures were drawn in ChemDraw 19.1.

5.2 Automated In-situ Photodosing Spectrometer.

Samples were exposed to ambient indoor conditions in June at NREL in Golden, CO with 120 mW/cm^2 light exposure of from a four bulb DC halogen lamp (Sylvania 58321) array. Samples were rotated continuously during photobleaching to ensure uniform exposure and absorption and reflection spectra were taken at set intervals. Multiples of films were placed on the system and were removed for separate analysis after different APDs to ensure both reproducibility in the measurements and to reduce the possibility of the decay rates being affected by experimentation or interruption. The fraction of light absorbed, or fractional absorptance (FA), spectra were calculated from the fraction reflected (FR) and fraction transmitted (FT) as FA=1-FT-FR. FT and FR spectra were collected by separate spectrometers (Ocean Optics HR2000) fitted with a collimating lens and a 'six around one' reflectance probe, respectively. The accumulated photon dose (APD) was calculated using equation 1:

$$APD(t_i) = \int_{t=t_0}^{t=t_i} \int_{\lambda_1}^{\lambda_2} FA(\lambda, t) \cdot I_{L_{photon}}(\lambda) d\lambda dt \quad (1)$$

Where $I_{L_{photon}}$ is the lamp array's spectral photon flux. A six-inch integrating sphere (Optronic Labs OL IS-670) fitted with silicon (Soma S-2441C) and InGaAs (Spectral evolution LF1250) diode arrays was used to gather the spectral irradiance data of the photobleaching light source which was converted to photon flux using equation 2:

$$I_{L_{photon}}(\lambda) = \frac{Spectralirradiance(\lambda) * \lambda}{hc} \quad (2)$$

5.3 Grazing-Incidence Wide-Angle X-ray Scattering.

GIWAXS experiments were carried out at the Stanford Synchrotron Radiation Lightsource (SSRL) on beamline 11-3 which is equipped with a two-dimensional Rayonix MX225 CCD area detector. A beam energy of 12.7 keV and an incident angle of measurement of ~0.12° were used. A LaB6 standard sample was used to calibrate the wavelength and sample-detector distance. The two-dimensional detector images were converted from intensity vs pixel position to intensity vs reciprocal space (q-space) in Igor 6.37 using WAXS tools and Nika macros. [64] The two-dimensional images were converted to one-dimensional intensity vs q_z- and q_{xy}-space by integration of chi segments taken from chi of 0-15° and 73-88°, respectively.

5.4 X-ray Photoelectron Spectroscopy.

Polymer samples were spincast onto indium tin oxide (ITO) substrates approximately 1 cm x 1 cm for XPS. The experiment was performed with a Kratos Axis Ultra X-ray photoelectron spectrometer utilizing a 1486.6 eV monochromatic Al Kα source at a base pressure of 10^{-8} Torr. Photoelectrons were collected and analyzed using a hemispherical analyzer and a photodiode array and a 20 eV pass energy was used for all element specific acquisitions. The resulting regional spectra were background corrected using the Shirley function. Quantifications of percent atomic concentration were done by area.

Author Contributions

MAA: conceptualization, methodology, investigation, visualization, formal analysis, project administration, writing – original draft, and writing – review & editing. AH: methodology and writing – review & editing. BWL: conceptualization, supervision, data curation, resources, writing – review & editing, and funding acquisition. ELR: conceptualization, supervision, visualization, resources, and writing – review & editing, and funding acquisition.

Conflicts of interest

There are no conflicts to declare.

Acknowledgements

The authors would like to thank Dr. John C. Jewett (Department of Chemistry and Biochemistry, University of Arizona) for insights and guidance regarding chemical products and their formation pathways. MAA, AH, and ELR were supported by the National Science Foundation under grant award DMR-2003631. MAA acknowledges support from the ARCS foundation. Use of the Stanford Synchrotron Radiation Lightsource, SLAC National Accelerator Laboratory, is supported by the U.S. Department of Energy, Office of Science, Office of Basic Energy Sciences under Contract No. DEAC02-76SF00515. A portion of this work was conducted in the Nano Fabrication Center at the University of Arizona. This work was authored in part by the National Renewable Energy Laboratory, operated by Alliance for Sustainable Energy, LLC, for the U.S. Department of Energy (DOE) under Contract No. DE-AC36-08GO28308 through the ARPA-E DIFFERENTIATE program under grant no. DE-AR0001215. The views expressed in the article do not necessarily represent the views of the DOE or the U.S. Government.

Notes and references

1. E. T. Hoke, I. T. Sachs-Quintana, M. T. Lloyd, I. Kauvar, W. R. Mateker, A. M. Nardes, C. H. Peters, N. Kopidakis and M. D. McGehee, *Adv. Energy Mater.*, 2012, **2**, 1351.
2. T. Wang, T. R. Kafle, B. Kattel and W.-L. Chan, *Journal of the American Chemical Society*, 2017, **139**, 4098-4106.
3. M. Knupfer, *Applied Physics A*, 2003, **77**, 623-626.

4. F. Bureš, *RSC Adv.*, 2014, **4**, 58826-58851.
5. J. Roncali, *Chemical Reviews*, 1997, **97**, 173-206.
6. H. Bronstein, C. B. Nielsen, B. C. Schroeder and I. McCulloch, *Nat. Rev. Chem.*, 2020, **4**, 66.
7. Best Research-Cell Efficiency Chart, https://www.nrel.gov/pv/cell-efficiency.html).
8. H. Zhou, L. Yang and W. You, *Macromolecules*, 2012, **45**, 607-632.
9. C. Han, J. Wang, S. Zhang, L. Chen, F. Bi, J. Wang, C. Yang, P. Wang, Y. Li and X. Bao, *Advanced Materials*, 2023, **35**, 2208986.
10. D. G. Farnum, G. Mehta, G. G. I. Moore and F. P. Siegal, *Tetrahedron Letters*, 1974, **15**, 2549-2552.
11. Y. Liang, D. Feng, Y. Wu, S.-T. Tsai, G. Li, C. Ray and L. Yu, *Journal of the American Chemical Society*, 2009, **131**, 7792-7799.
12. J. Min, Z.-G. Zhang, S. Zhang and Y. Li, *Chemistry of Materials*, 2012, **24**, 3247-3254.
13. Q. T. Zhang and J. M. Tour, *Journal of the American Chemical Society*, 1998, **120**, 5355-5362.
14. D. Qian, L. Ye, M. Zhang, Y. Liang, L. Li, Y. Huang, X. Guo, S. Zhang, Z. A. Tan and J. Hou, *Macromolecules*, 2012, **45**, 9611-9617.
15. L. Huo, J. Hou, S. Zhang, H.-Y. Chen and Y. Yang, *Angewandte Chemie International Edition*, 2010, **49**, 1500-1503.
16. C. Gao, L. Wang, X. Li and H. Wang, *Polym. Chem.*, 2014, **5**, 5200-5210.
17. Y. Li, P. Sonar, L. Murphy and W. Hong, *Energy Environ. Sci.*, 2013, **6**, 1684.
18. W. Zhuang, S. Wang, Q. Tao, W. Ma, M. Berggren, S. Fabiano, W. Zhu and E. Wang, *Macromolecules*, 2021, **54**, 970-980.
19. L. Dou, J. You, J. Yang, C.-C. Chen, Y. He, S. Murase, T. Moriarty, K. Emery, G. Li and Y. Yang, *Nature Photonics*, 2012, **6**, 180-185.
20. Y. Liang and L. Yu, *Accounts of Chemical Research*, 2010, **43**, 1227-1236.
21. S.-H. Liao, H.-J. Jhuo, Y.-S. Cheng and S.-A. Chen, *Advanced Materials*, 2013, **25**, 4766-4771.
22. S. Zhang, L. Ye, W. Zhao, D. Liu, H. Yao and J. Hou, *Macromolecules*, 2014, **47**, 4653-4659.
23. F. Bencheikh, D. Duché, C. M. Ruiz, J.-J. Simon and L. Escoubas, *The Journal of Physical Chemistry C*, 2015, **119**, 24643-24648.
24. J.-D. Chen, C. Cui, Y.-Q. Li, L. Zhou, Q.-D. Ou, C. Li, Y. Li and J.-X. Tang, *Advanced Materials*, 2015, **27**, 1035-1041.
25. Z. Genene, J. Wang, X. Meng, W. Ma, X. Xu, R. Yang, W. Mammo and E. Wang, *Advanced Electronic Materials*, 2016, **2**, 1600084.
26. Z. Zheng, H. Yao, L. Ye, Y. Xu, S. Zhang and J. Hou, *Materials Today*, 2020, **35**, 115-130.
27. L. Zhan, S. Li, Y. Li, R. Sun, J. Min, Y. Chen, J. Fang, C.-Q. Ma, G. Zhou, H. Zhu, L. Zuo, H. Qiu, S. Yin and H. Chen, *Advanced Energy Materials*, 2022, **12**, 2201076.
28. W. Liu, S. Xu, H. Lai, W. Liu, F. He and X. Zhu, *CCS Chemistry*, 2023, **5**, 654-668.
29. X. Zhu, S. Liu, Q. Yue, W. Liu, S. Sun and S. Xu, *CCS Chemistry*, 2021, **3**, 1070-1080.
30. W. R. Mateker and M. D. McGehee, *Adv. Mater.*, 2017, **29**, 1603940.
31. A. Perthue, I. F. Dominguez, P. Verstappen, W. Maes, O. J. Dautel, G. Wantz and A. Rivaton, *Solar Energy Materials and Solar Cells*, 2018, **176**, 336-339.
32. S. Chambon, A. Rivaton, J.-L. Gardette and M. Firon, *Journal of Polymer Science Part A: Polymer Chemistry*, 2009, **47**, 6044-6052.
33. H. Usta, C. Risko, Z. Wang, H. Huang, M. K. Deliomeroglu, A. Zhukhovitskiy, A. Facchetti and T. J. Marks, *Journal of the American Chemical Society*, 2009, **131**, 5586-5608.
34. L. Ma, X. Wang, B. Wang, J. Chen, J. Wang, K. Huang, B. Zhang, Y. Cao, Z. Han, S. Qian and S. Yao, *Chemical Physics*, 2002, **285**, 85-94.
35. E. M. Speller, A. J. Clarke, N. Aristidou, M. F. Wyatt, L. Francàs, G. Fish, H. Cha, H. K. H. Lee, J. Luke, A. Wadsworth, A. D. Evans, I. McCulloch, J.-S. Kim, S. A. Haque, J. R. Durrant, S. D. Dimitrov, W. C. Tsoi and Z. Li, *ACS Energy Letters*, 2019, **4**, 846-852.
36. K. E. Watts, T. Nguyen, B. J. T. d. Villers, B. Neelamraju, M. A. Anderson, W. A. Braunecker, A. J. Ferguson, R. E. Larsen, B. W. Larson, Z. R. Owczarczyk, J. R. Pfeilsticker, J. E. Pemberton and E. L. Ratcliff, *J. Mater. Chem. A*, 2019, **7**, 19984.
37. I. E. Brumboiu, L. Ericsson, R. Hansson, E. Moons, O. Eriksson and B. Brena, *J. Chem. Phys.*, 2015, **142**, 054306.
38. H. Hintz, H. J. Egelhaaf, H. Peisert and T. Chassé, *Polym. Degrad. Stab.*, 2010, **95**, 818.
39. J. Kettle, Z. Ding, M. Horie and G. C. Smith, *Organic Electronics*, 2016, **39**, 222.
40. J. Kettle, H. Waters, Z. Ding, M. Horie and G. C. Smith, *Sol. Energy Mater. Sol. Cells*, 2015, **141**, 139.
41. M. Manceau, J. Gaume, A. Rivaton, J.-L. Gardette, G. Monier and L. Bideux, *Thin Solid Films*, 2010, **518**, 7113-7118.
42. S. Kim, M. A. M. Rashid, T. Ko, K. Ahn, Y. Shin, S. Nah, M. H. Kim, B. Kim, K. Kwak and M. Cho, *The Journal of Physical Chemistry C*, 2020, **124**, 2762-2770.
43. L. E. Garner, V. Nellissery Viswanathan, D. H. Arias, C. P. Brook, S. T. Christensen, A. J. Ferguson, N. Kopidakis, B. W. Larson, Z. R. Owczarczyk, J. R. Pfeilsticker, P. C. Ramamurthy, S. H. Strauss, O. V. Boltalina and W. A. Braunecker, *J. Mater. Chem. A*, 2018, **6**, 4623.
44. M. A. Anderson, B. W. Larson and E. L. Ratcliff, *ACS Applied Materials & Interfaces*, 2021, **13**, 44641-44655.
45. X. Huang, L. Zhang, Y. Cheng, J. Oh, C. Li, B. Huang, L. Zhao, J. Deng, Y. Zhang, Z. Liu, F. Wu, X. Hu, C. Yang, L. Chen and Y. Chen, *Advanced Functional Materials*, 2022, **32**, 2108634.
46. F.-C. Hsu, J.-W. Luo, Y.-W. Su, C.-S. Yang, Y.-A. Lin, J.-Y. Lin, C.-Y. Chang, Y.-F. Chen and C.-P. Li, *ACS Applied Energy Materials*, 2020, **3**, 4217-4225.
47. T. Kim, J.-H. Kim, T. E. Kang, C. Lee, H. Kang, M. Shin, C. Wang, B. Ma, U. Jeong, T.-S. Kim and B. J. Kim, *Nature Communications*, 2015, **6**, 8547.
48. F. C. Löhrer, C. Senfter, C. J. Schaffer, J. Schlipf, D. Moseguí González, P. Zhang, S. V. Roth and P. Müller-Buschbaum, *Advanced Photonics Research*, 2020, **1**.
49. A. Rivaton, A. Tournebize, J. Gaume, P.-O. Bussière, J.-L. Gardette and S. Therias, *Polymer International*, 2014, **63**, 1335-1345.
50. Y. Kaptan, Ö. Pekcan, E. Arca and O. Güven, *Journal of Applied Polymer Science*, 1989, **37**, 2577-2585.

51. A. Dupuis, P. Wong-Wah-Chung, A. Rivaton and J.-L. Gardette, *Polymer Degradation and Stability*, 2012, **97**, 366-374.
52. A. Tournebize, J. L. Gardette, C. Taviot-Guého, D. Bégué, M. A. Arnaud, C. Dagron-Lartigau, H. Medlej, R. C. Hiorns, S. Beaupré, M. Leclerc and A. Rivaton, *Polym. Degrad. Stab.*, 2015, **112**, 175.
53. W. R. Mateker, T. Heumueller, R. Cheacharoen, I. T. Sachs-Quintana, M. D. McGehee, J. Warnan, P. M. Beaujuge, X. Liu and G. C. Bazan, *Chemistry of Materials*, 2015, **27**, 6345-6353.
54. D. E. Shen, A. W. Lang, G. S. Collier, A. M. Österholm, E. M. Smith, A. L. Tomlinson and J. R. Reynolds, *Chemistry of Materials*, 2022, **34**, 1041-1051.
55. A. Shyichuk and J. White, *Journal of Applied Polymer Science*, 2000, **77**, 3015-3023.
56. J. Kettle, Z. Ding, M. Horie and G. C. Smith, *Organic Electronics*, 2016, **39**, 222-228.
57. M. Grzybowski and D. T. Gryko, *Adv. Opt. Mater.*, 2015, **3**, 280.
58. J. Eng, I. A. Hubner, J. Barriocanal, R. L. Opila and D. J. Doren, *J. Appl. Phys.*, 2004, **95**, 1963.
59. K. Norrman, M. V. Madsen, S. A. Gevorgyan and F. C. Krebs, *J. Am. Chem. Soc.*, 2010, **132**, 16883.
60. M. Manceau, A. Rivaton, J.-L. Gardette, S. Guillerez and N. Lemaître, *Polymer Degradation and Stability*, 2009, **94**, 898-907.
61. T. Thiemann, IntechOpen, 2019, DOI: 10.5772/intechopen.79080.
62. T. Thiemann, *Journal of Chemical Research*, 2010, **34**, 665-679.
63. M. S. Sharifi, H. Douroudgari and M. Vahedpour, *Scientific reports*, 2021, **11**, 1-20.
64. S. D. Oosterhout, V. Savikhin, J. Zhang, Y. Zhang, M. A. Burgers, S. R. Marder, G. C. Bazan and M. F. Toney, *Chem. Mater.*, 2017, **29**, 3062.